ENGINEERING MATHEMATICS
AND COMPUTING LAB

UNIVERSITÄT
HEIDELBERG
ZUKUNFT
SEIT 1386

ACSeg: Automated 3D Cytoplasm Segmentation in Soft X-Ray Tomography

Ayse Aydogdu-Erozan, Philipp D. Lösel, Vincent Heuveline, Venera Weinhardt

Preprint No. 2023-02

Preprint Series of the Engineering Mathematics and Computing Lab (EMCL)

www.emcl.iwr.uni-heidelberg.de

Preprint Series of the Engineering Mathematics and Computing Lab (EMCL)
ISSN 2191–0693
Preprint No. 2023-02

Affiliation of the Authors

Ayse Aydogdu-Erozan[a, b, 1], Philipp D. Lösel[b], Vincent Heuveline[b], Venera Weinhart[a]

[a] *Centre for Organismal Studies (COS), Heidelberg University, Germany*
[b] *Engineering Mathematics and Computing Lab (EMCL), Interdisciplinary Center for Scientific Computing (IWR), Heidelberg University, Germany*
[1] *Corresponding Author: Ayse Aydogdu-Erozan, ayse.erozan@uni-heidelberg.de*

Impressum

Heidelberg University
Interdisciplinary Center for Scientific Computing (IWR)
Engineering Mathematics and Computing Lab (EMCL)

Im Neuenheimer Feld 205,
69120 Heidelberg
Germany

ACSeg: Automated 3D Cytoplasm Segmentation in Soft X-Ray Tomography

Ayse Aydogdu-Erozan, Philipp D. Lösel, Vincent Heuveline, Venera Weinhardt

April 4, 2023

Abstract

The structure of cells is a key to understanding cellular function, diagnosis of pathological conditions, and development of new treatments. Soft X-ray tomography (SXT) is a unique tool to image cellular structure without fixation or labeling at high spatial resolution and throughput. Ongoing improvements in faster acquisition times increase demand for accelerated image analysis. Currently, the automatic segmentation of cellular structures is a major bottleneck in the SXT data analysis pipeline. In this paper, we introduce an automated 3D cytoplasm segmentation model - ACSeg - by use of semi-automatically segmented labels and 3D U-Net, implemented in the online platform Biomedisa. The segmentation model is trained on semi-automatically labeled datasets and shows rapid convergence to high-accuracy segmentation, therefore reducing time and labor. ACSeg trained on 43 SXT tomograms of human immune T cells, the model successfully segmented unseen SXT tomograms of human hepatocyte-derived carcinoma cells, mouse microglia, and embryonic fibroblast cells. Furthermore, we could diversify the model by adding only 6 specific SXT tomograms, showing the potential for the development of an optimal experimental design. The ACSeg is published on the open image segmentation platform Biomedisa, enabling high-throughput analysis of cell volume and structure of cytoplasm in diverse cell types. The approach can be expanded for automatic segmentation of other organelles visualized by SXT, providing means for structural analysis of cell remodeling under different pathogens at statistically significant sizes, therefore enabling the development of novel drug treatments.

1 Introduction

The analysis of structure is a fundamental task in cell biology, as the size, shape, and internal anatomy of cells alter to enable new functions and adapt to changing environments, including pathological conditions [1, 2]. Various disorders such as cancer, malaria, anemia [1], and sickle cell disease [3] result in abnormal cell shape. With this in mind, determining the three-dimensional shape of cells is one of the most important aspects of cell biology[4].

Thus many microscopy techniques have been focused on imaging and analysis of the cell structure [5, 6, 7]. Among existing imaging techniques, soft x-ray tomography (SXT) enables imaging of whole mammalian cells with a spatial resolution of a few tens of nanometers, without labeling or chemical fixation, and at high throughput of 5 min for whole 3D volume [8]. While segmentation pipelines for light and electron microscopy are firmly established, automatic analysis of SXT data is limited [9].

Most of the SXT-based structural cell analysis is based on manual segmentation [8, 10, 11, 12]. Thresholding-based segmentation methods which require no prior labeled data have been proposed to extract mitochondria and cytoplasmic vesicles in Nahas et al. study [13, 14]. Cossa et al. [15] applied random forest segmentation to extract nucleoids from Escherichia coli. To extract mitochondria, Polo et al. [16] implemented a trainable weka segmentation machine learning tool [17], accessible in Fiji. Furthermore, neural network-based algorithms, such as convolutional neural networks (CNN) or U-Net, have been used to extract membranous organelles in Dyhr et al [9], Francis et al.[18] and Egebjerg et al. [19] study.

A segmentation method based on the combination of 2D U-Nets was used to automatically segment whole β-cells anatomy [20]. Most of these methods are designed for a very specialized organelle type or pathological condition and automatic segmentation of whole cell anatomy requires complex pre- and post-processing steps.

Here, we propose an easy plug-and-play model (ACSeg) based on 3D U-Net to extract the cell cytoplasm structure in various cell types. We exploit the semi-automatic segmentation based on 3D random walk implemented in the open platform Biomedisa [21]. Apart from minimizing the time for manual segmentation [22], our results show that the high-quality of segmented labels enables us to train the 3D U-Net on only 20 tomograms to achieve a dice coefficient of 95.43%. Moreover, even though ACSeg was trained exclusively on tomograms containing human T-cells, ACSeg was able to segment cell cytoplasm of 4 unseen cell types with a dice coefficient of about 87.62%. This accuracy could be significantly improved with only additional 6 tomograms, diversifying ACSeg for automatic segmentation of various cell types. Interestingly, our data shows that the success of ACSeg diversification depends on the type of cells and/or data quality, suggesting that optimal experimental design should be in focus for the training of 3D U-Nets. Overall, the ACSeg enables fast and accurate cell cytoplasm segmentation of diverse cells imaged with SXT. Published as plug and play model in the online Biomedisa application, it enables analysis of changes in cell cytoplasm under different pathological conditions of various cells without pre-processing of SXT data. With the development of the lab-based SXT [23] and increasing use of SXT in viral research and development of novel drugs, the ACSeg is an important step toward fully automatic analysis of cell structure.

2 Material and Methods

2.1 Soft-X-ray tomography

SXT imaging was performed at the XM-2 beamline of the Advanced Light Source at the Lawrence Berkeley National Laboratory [24]. We have used a 60 nm outermost zone width Fresnel Zone plate to image cells in full rotation tomography [25]. The cells were mixed with polystyrene beads, and plunge frozen in thin-wall glass capillaries and 92 x-ray projection images were acquired over 180° rotation with an exposure time of 200 ms. The 3D reconstructions of cells were obtained with AREC3D [26]. Further experimental details can be found elsewhere [27].

2.2 Dataset

On average, the tomograms have dimensions of 472 $\times$ 472 $\times$ 491 voxels with slight variability due to shifting of the capillary in the x-ray beam and thus a variable field of view [26]. The 53 tomograms of T cells are randomly divided into two partitions 80% to 20%: 43 for training, and 10 for testing of the network.

The dataset for testing the accuracy of divergent cell types consisted of a total of 39 tomograms containing four different cell types: 12 Huh-7, 12 BV-2, 9 MEF, and 3 β-cells [20, 28]. In order to generalize the training dataset, 6 additional tomograms containing Huh-7, BV-2, and MEF cells individually were added to the training dataset in 3 different retraining. Briefly, a total of 54 tomograms were used for the entire generalization process, which means that another 18 tomograms were used for training, and 39 were used for testing.

2.3 Semi-Automated Labeling

To generate ground truth, testing datasets were manually segmented with Slicer3D using the segment editor tool [29, 30]. Similarly, we have performed manual segmentation of 43 tomograms used for training. For training, we decided to use Biomedisa which is an open-source online platform, to segment 3D volumes based on smart interpolation of sparsely segmented slices [22]. To generate 3D masks semi-automatically, labels were assigned manually to cell cytoplasm and polystyrene beads in every 20th slice. These sparsely labeled slices were submitted to Biomedisa for smart interpolation to obtain labels of whole 3D volume. If the generated 3D labels were mislabeled or the quality to the naked eye was insufficient, we added a few

manually labeled slices. From 43 tomograms used in this work, 95 percent were segmented with 20±3 manually labeled slices, and for 5 percent 3D tomograms 30±3 slices were required to obtain 3D labels.

2.4 Model Training

In this work, we applied 3D U-net integrated into the online platform Biomedisa. This implementation of the 3D U-net is one level deeper than classical 3D U-net [31]. Details on the network architecture and parameters used in the 3D U-net of Biomedisa can be found elsewhere [22]. The model was trained on 43 SXT tomograms containing a different number of T cells and polystyrene beads with the following parameters: 200 epochs, a batch size of 24, and a learning rate of 0.01. The training data were split (80%) and (20%) for training and self-validation of the network as controlled by the Biomedisa parameter settings. The best network is achieved after 33 hours.

3 Results

3.1 Automatic segmentation workflow for cell cytoplasm

To train our U-Net model for cytoplasm segmentation in SXT data, it is first necessary to generate 3D labels. In order to reduce manual work, we used Biomedisa for semi-automatic 3D segmentation [22]. We manually labeled every 20th slice in tomograms and submitted labels to Biomedisa for generating 3D labels by using smart interpolation, see Figure 1. By use of semi-automatic labeling, we reduced the amount of manual work required to train the model by 94.6 percent compared to fully manual segmentation. The generated 3D labels along with 3D tomograms were used to train our U-Net model, implemented within Biomedisa for the automatic segmentation of cell cytoplasm. The segmentation workflow is summarized in Figure 1, where the trained network is depicted as ACSeg for the automatic cytoplasm segmentation.

3.2 Evaluation of ACSeg

Previous work on U-Net segmentation showed that the number and quality of training datasets are crucial to achieving high accuracy of segmentation [32, 33]. Therefore, we have measured the accuracy of the ACSeg by computing Dice coefficients [34, 35] for U-net trained on various SXT tomograms. We trained the ACSeg on 5, 10, 20, 30, and 43 datasets, see Table 1 and Figure 2. With only 20 training datasets, our ACSeg achieved a dice coefficient above 95 %. We have investigated whether such fast convergence of dice coefficient is due to the higher quality of semi-automatic segmentation in the prediction of labels which was mentioned in insect studies [32]. We have compared the ACSeg trained on manually segmented labels in comparison to semi-automatically with Biomedisa. The ACSeg trained on the manual labels showed a lower dice coefficient for 5 training datasets with 87 % accuracy compared to 90 % with ACSeg trained on 3D labels from Biomedisa, see Figure 2. Interestingly, this relatively low difference of 3 % in accuracy is not compensated by the increased number of tomograms. ACSeg trained on 43 datasets results in 94 % for manually labeled data and 98 % for Biomedisa labeled data. We have fitted the so-called 1st order delay function, that is $1 - b \cdot \exp(-ax)$, to find the number of manually labeled tomograms required to achieve 98 % accuracy. This approximation shows that about 52 additional manually segmented tomograms (95 in total) would be required to achieve the same accuracy as ACSeg trained on 43 semi-automatically segmented datasets.

For ACSeg trained on Biomedisa results, adding 10 datasets increases the accuracy at first steeply but then only gradually with more than 20 datasets, suggesting that the addition of more datasets is unnecessary. It has been shown that choosing the dice coefficient as a performance metric is often not an adequate measure for training models [35]. To assess the performance of the ACSeg from the biological perspective, we calculated two major parameters used in cell biology to normalize for cell variability and change of structure, that is volume and surface-to-volume ratio of cells [10]. We found no significant difference in volume (Figure 3A) compared between ground truth (generated with Biomedisa) by producing Biomedisa and ACSeg predictions. On the contrary, the probability for the surface-to-volume ratio is only 0.001478 (Figure 3B). Consistent with this, we found differences in the cytoplasmic morphology that are noticeable in 3D renderings (Figure $3C_3$-$3C_4$). Many cells have cytoplasmic projections with fine

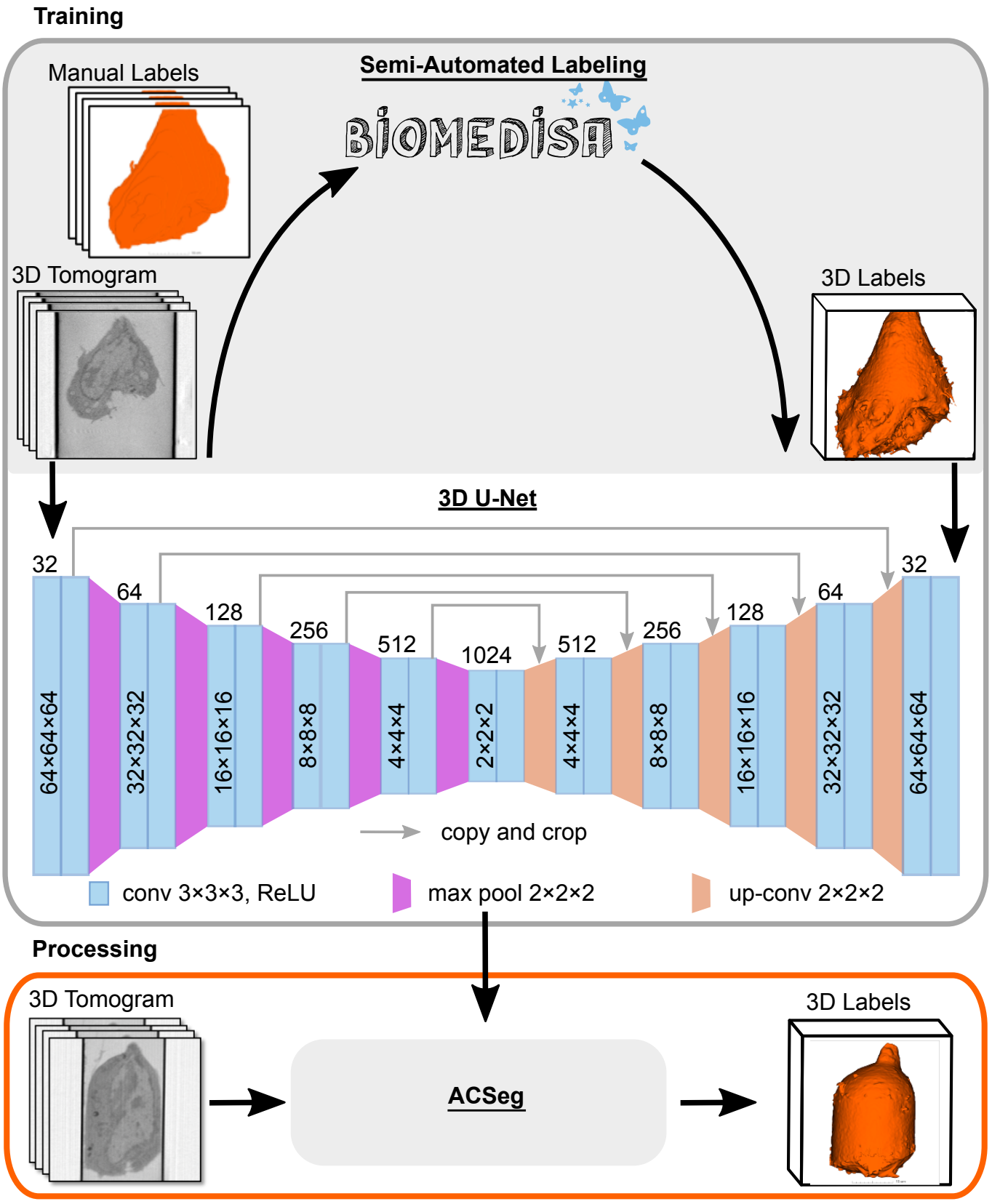

Figure 1: Automated cytoplasm segmentation workflow with semi-automated labeling

Table 1: The effect of alteration of the number of tomograms for training on the dice coefficient of the model

# of cells for training	Dice coefficient, %	
	Biomedisa labels	Manual labels
5	90.03 ± 15.61	86.81 ± 30.90
10	94.22 ± 15.33	87.69 ± 17.48
20	95.43 ± 11.94	90.93 ± 12.72
30	96.17 ± 11.00	92.61 ± 10.37
43	97.78 ± 2.13	93.87 ± 7.37

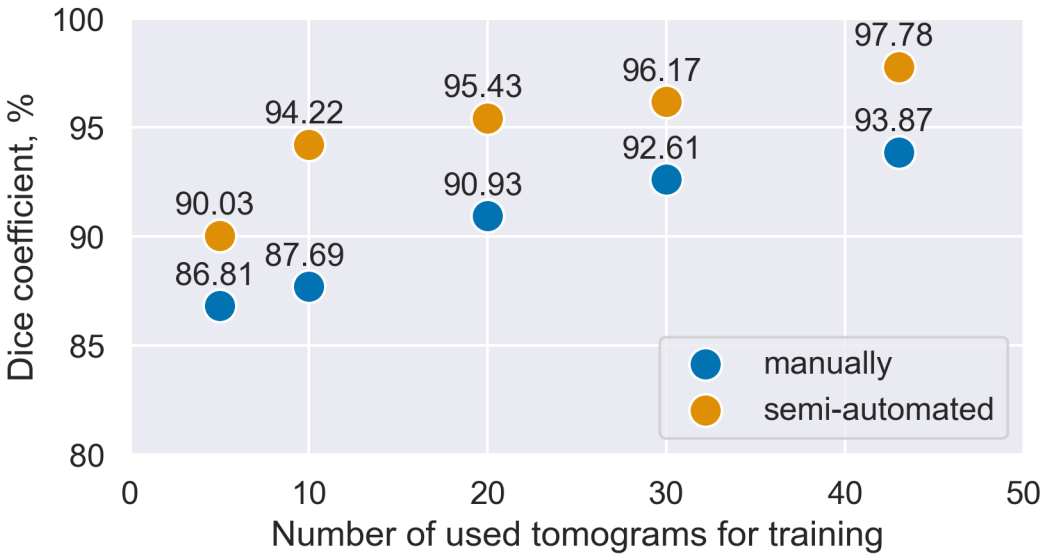

Figure 2: Dice coefficient according to alteration of the number of the training data

ultrastructure which is hard to detect automaticaly. Noticeably, the ACSeg segmentation did not predict the ultrastructure of some filopodia in comparison to the ground truth. We believe that the reason behind the low surface-to-volume ratio is that there is a considerable loss in surface resolution due to dataset scaling. In conclusion, the ACSeg trained on 43 datasets is sufficient to successfully predict the gross cell volume and most of the filopodia, which are sufficient for morphological analysis where cell volume is used for normalization and visual structural representation used in cell biology.

3.3 Comparison of ACSeg to other approaches

Intuitively, one could think that cytoplasm segmentations in the SXT data should be easy to capture by conventional approaches, such as thresholding. It is worth mentioning that the content of SXT tomograms varies a lot. For SXT imaging, cells are suspended in thin-wall glass capillary inside the microscope [27]. Many cells are touching the capillary wall. Additionally, polystyrene beads are added for SXT normalization in the imaging of large cells. Their distribution is random and not consistent between tomograms. The biology of cells starts to play a role as well. Some cells are apoptotic with fragments of their cytoplasm visible in SXT tomograms. All these effects are stochastic and can not be controlled in the SXT experiments. To demonstrate this effect, we show 4 cases in Figure 4: an isolated cell with debris from other cells, a cell touching the glass capillary, cells tightly packed in the capillary, and a cell between two polystyrene beads. We have used thresholding methods, such as the adaptive and Otsu thresholding, which do not perform well in segmentation in most cases, see Figure 4. While these methods can be

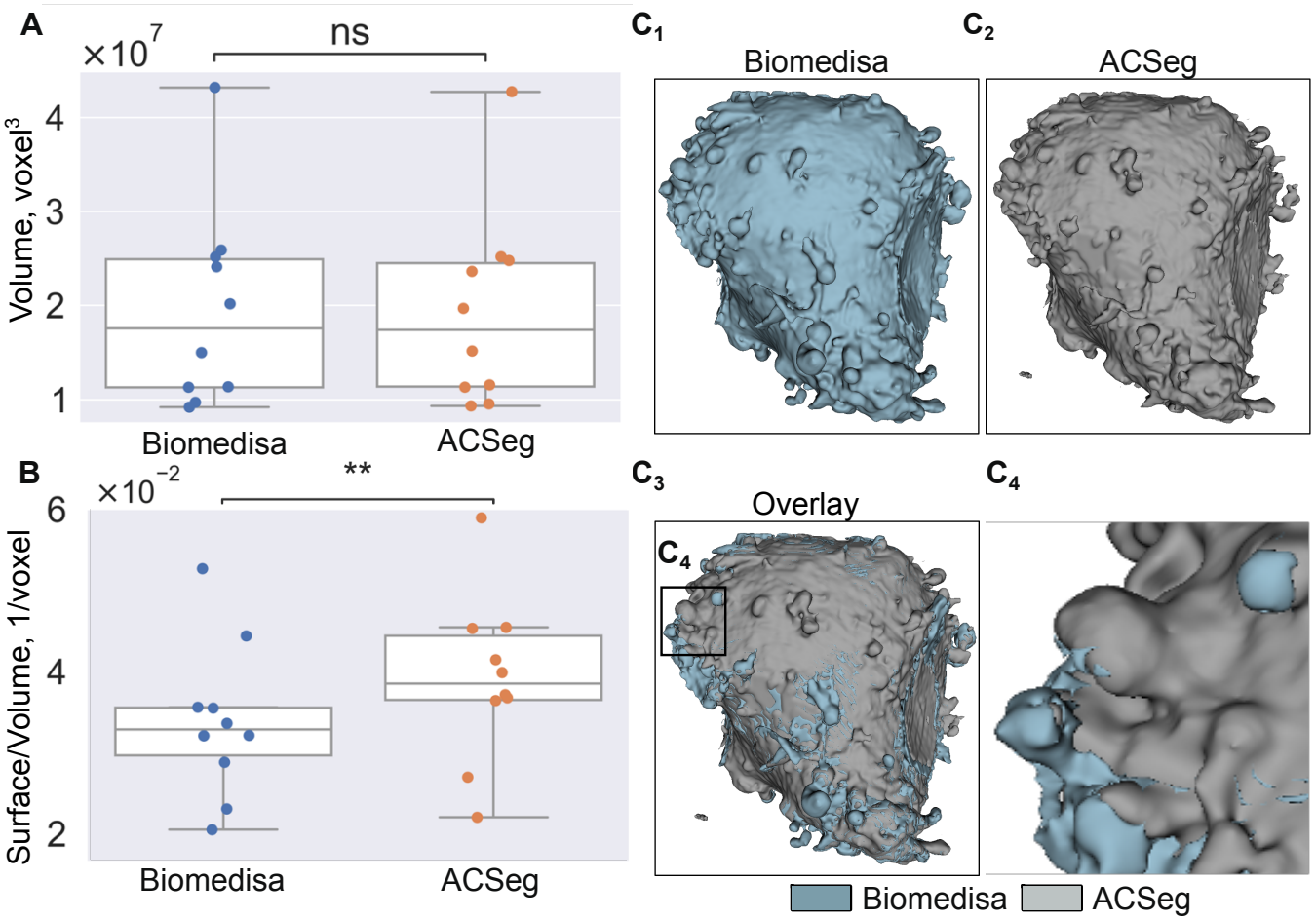

Figure 3: ACSeg segmentation and morphological quantification of T cells. The volume (A) and surface area to volume ratio (B) of the cell were measured in the ground truth and prediction of cytoplasm segmentation with the ACSeg. $ns : p>0.05, * : 0.01<p<=0.05, ** : 0.001<p<=0.01$, using paired t-test. N = 10. C) 3D rendering of Biomedisa (C1) and prediction of the ACSeg (C2) respectively, visual comparison of Biomedisa and our model's prediction(C3).

optimized with pre- and post-processing to increase segmentation quality, such an optimization pipeline would need to be adjusted to individual cases. The ACSeg segmentation of these difficult cases remains accurate without any pre- and post-processing steps.

3.4 ACSeg transfer to other cell types

Because the cells are so diverse in size and morphology, it is typically difficult to apply a segmentation network trained on one type of cells to others. We therefore first tested our model on the open SXT datasets of β-cells (INS-1E - a rat insulinoma cell line). Li et al. already segmented cytoplasm and some organelles [20]. Comparing cytoplasm segmentation, we achieved 95.31 $\pm$ 5.59 % dice coefficient for 3 tomograms which is slightly better than the results from Li's study (dice coefficient of 91.60 $\pm$ 2.19 %).

To test even more divergent cell types, we have tested ACSeg on SXT datasets of hepatocyte-derived carcinoma Huh-7, murine microglia BV-2, and mouse embryonic fibroblasts MEF cells, see Table II. For MEF cells, the ACSeg showed high accuracy with 94.43% measured by the dice coefficient. The segmentation of Huh-7 and BV-2 cells, however, was not successful with 82.93 % and 84.06 % dice coefficients respectively. To see whether ACSeg will have higher accuracy by generalization of training datasets, we included other cell types. We have added to 43 3D labels of T cells, 3D labels of 6 SXT

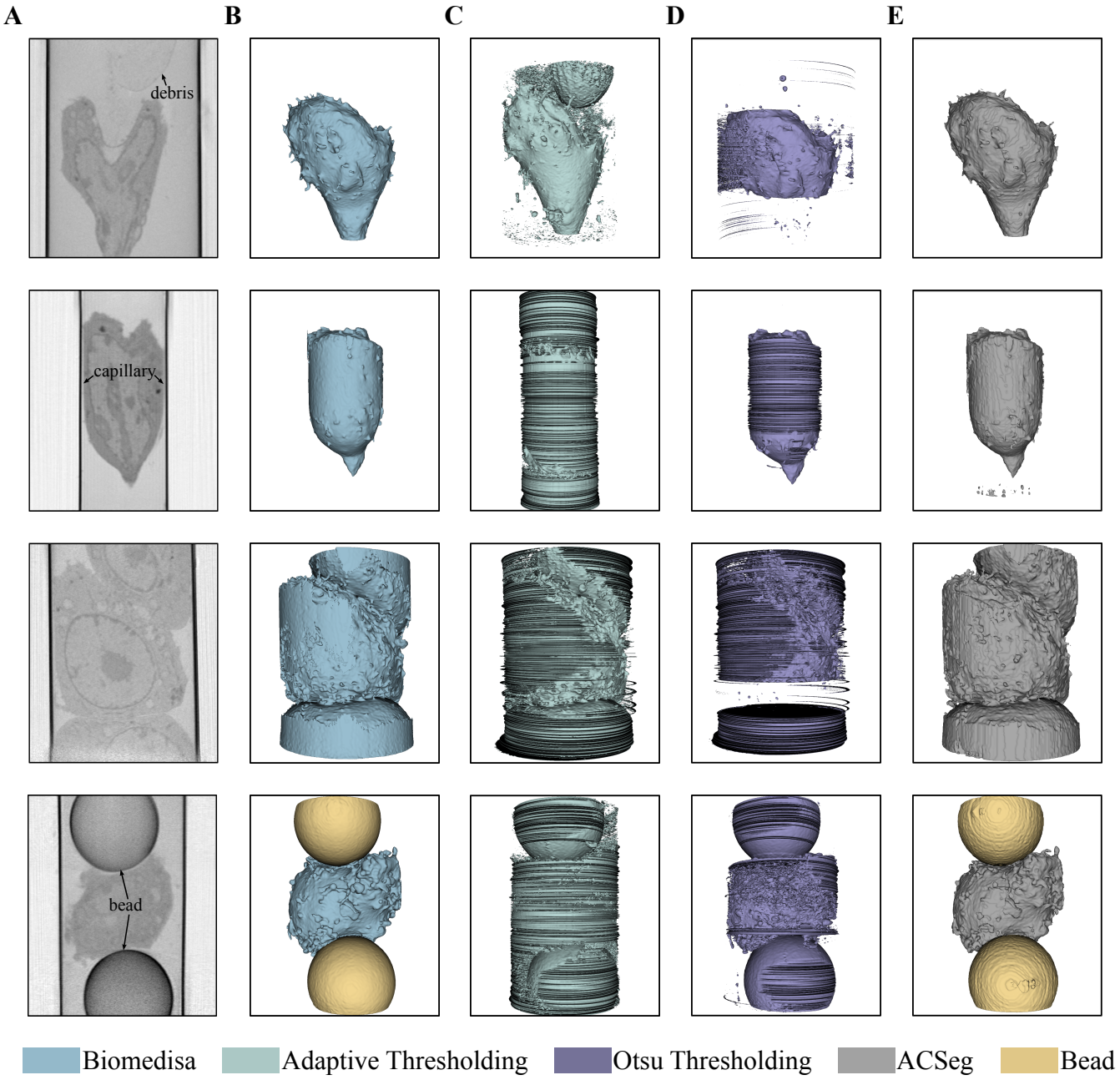

Figure 4: Quantification of Cytoplasm Segmentation Accuracy. A) A representative example 2D slice from the 3D tomogram that was tested. 3D rendering of the Biomedisa results(B), adaptive threshold results (C), otsu threshold results (D), and our method results (E), respectively.

tomograms for Huh-7 cells to our training data. Interestingly with the addition of such a small number of data, the retrained ACSeg showed a 10 % increase not only for Huh-7 cells but also for BV-2 cells. We explored whether ACSeg can be as successfully generalized by using an equivalent number of training datasets from BV-2 cells. The ACSeg trained on 43 3D labels of T cells and 6 BV-2 cells showed lower accuracy than generalization with Huh-7 cells with dice coefficient of 90.25%, 87.67%, and 94.58% for BV-2, Huh-7, and MEF cells correspondingly. Similarly we generalized ACSeg by the addition of 6 MEF cells and a mixture of Huh-7, BV-2, and MEF cells (6 tomograms each). Although both retraining processes

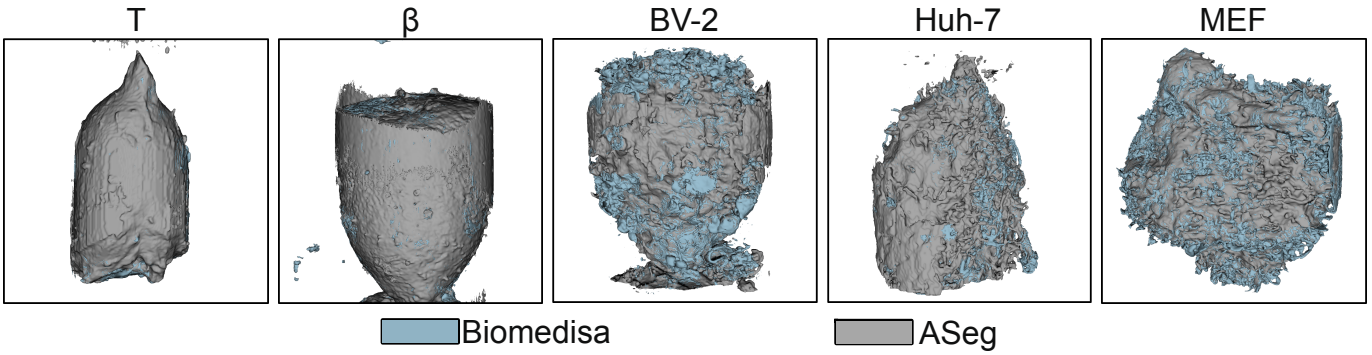

Figure 5: Prediction of the ACSeg over T, β, BV-2, Huh-7 and MEF cells

provided to increase in the overall dice coefficient, they, however, have not reached the success obtained from the network trained by combining 43 T cells with 6 Huh-7. The experiments revealed that the best accuracy measured by the dice coefficient was ACSeg trained on 43 T cells and 6 Huh-7 cells. Based on 3D labels segmented by ACSeg and Biomedisa (Figure 5), we can say that Huh-7 cells are more similar in number and structure of filopodia to BV-2 than T cells. However, at the moment we have no explanation why the generalization of the ACSeg on BV-2 cells does not increase accuracy on the same scale for Huh-7 cells or independent of ACSeg generalization the same accuracy is achieved for MEF cells. Possible metrics affecting the generalization of the ACSeg are under investigation.

Table 2: Accuracy results of ACSeg and its variants on divergent cell types

# of tomograms for training	Dice coefficient, %		
	BV-2 (12)	Huh-7 (12)	MEF (9)
43 (T cell)	83.19 ± 30.52	85.01 ± 23.98	94.43 ± 7.04
43 (T cell)+ 6 (BV-2 cell)	90.25 ± 13.90	87.67 ± 27.89	94.58 ± 6.21
43 (T cell) + 6 (Huh-7 cell)	95.49 ± 1.57	94.90±10.95	94.56 ± 7.45
43 (T cell) + 6 (MEF cell)	88.95 ± 17.72	86.76 ± 24.51	94.80 ± 7.07
43 (T cell) + 6 (Huh-7 cell) + 6 (BV-2 cell) + 6 (MEF cell)	92.82 ± 12.70	90.61 ± 31.29	94.74 ± 6.73

4 Discussion

Our work presents a pipeline for training a 3D U-Net on semi-automatically segmented SXT datasets for robust automatic segmentation of the cellular cytoplasm (ACSeg). Since ML and deep learning algorithms rely heavily on accurately labeled data that require expert knowledge, extensive time, and effort to train, we investigated a semi-automated segmentation approach using Biomedisa to generate increased quality of labeled training data for a 3D U-Net, generating a model that can segment the cytoplasm with high accuracy of more than 95 % within 1 minute. The use of labels generated with Biomedisa, provides faster convergence in training to higher dice coefficient compared to manual segmentation. These results illustrate that the quality of the labeling in the training dataset for the 3D cytoplasm segmentation is an important factor to achieve decent dice coefficient with less training data.

Even though we achieved a high dice coefficient with our model, we did not rely only on this pixel-wise

metric. In biology, segmented images are mostly used for statistical analysis of cell morphology. For this reason, we compared volume and surface-to-volume ratio as evaluation metrics as well. While the cell volume obtained with ACSeg is accurately measured, the surface-to-volume ratio of cells is not accurate. We believe this is due to build in scaling of tomograms to a size of 256 $\times$ 256 $\times$ 256 voxels. To achieve higher accuracy for fine features of the cell cytoplasm, alternative architectures such as Double U-Net should be considered [36]. Such an approach will help to improve the segmentation of fine features without a drastic increase in time for model training.

Although our model was trained on tomograms containing only one cell type, we have applied it to other cells of distinct morphology. Without any pre-processing methods, ACSeg showed high accuracy of more than 95 % for β-cells and mouse embryonic fibroblasts (MEF) cells [20]. For cells with lower accuracy, such as mouse microglia (BV-2) and epatocyte-derived carcinoma cells (Huh-7) cells, we generalize ACSeg with addition of a very small number of datasets in the training. Interestingly, the results show that there is cell-type (or dataset) specific success of model generalization. We expect that identifying optimal experimental design in terms of image quality and cell type should enable the development of automatic segmentation models based on small number of datasets.

5 Conclusion

In this paper, we described an automatic segmentation method based on a 3D U-net and a semi-automated labeling tool - Biomedisa - to automatically segment the cytoplasm of cells in SXT data with our novel ACSeg. The approach minimizes time and labor for the training of the model. We demonstrate that our test accuracy reaches more than 95% for T cells. By adding several tomograms of other cell types, we improved the performance of the ACSeg and demonstrated its generalization. The ACSeg is published as a free and easy-to-use model within Biomedisa. Without any pre-processing, it can be used for automatic and accurate segmentation of cell cytoplasm, enabling structural analysis and normalization of other cell metrics to cell volume. In the future, we envision extending such automatic segmentation of SXT data to other distinguishable organelles, like nuclei, mitochondria, and lipid droplets.

6 Acknowledgement

The work was funded within the framework of the Excellence Strategy of the Federal and State Governments of Germany and by the CoCID project (no. 101017116) funded within EU Research and Innovation Act. We thank Anthoula Chatzimpinou (COS, Heidelberg University), Maija Vihinen-Ranta (University of Jyväskylä, Finland), and Kate White (University of Southern California, USA) for providing the datasets. We are grateful to Axel Ekman, AG Wittbrodt (COS, Heidelberg University), Alexander Zeilmann, and Carolyn Larabell for their fruitful discussions and feedback on this research.

References

[1] Venera Weinhardt, Jian-Hua Chen, Axel Ekman, Gerry McDermott, Mark A Le Gros, and Carolyn Larabell. Imaging cell morphology and physiology using x-rays. *Biochemical Society Transactions*, 47(2):489–508, 2019.

[2] Joel Michael. What do we mean when we talk about "structure/function" relationships?, 2021.

[3] Michele C Darrow, Yujin Zhang, Bertrand P Cinquin, Elizabeth A Smith, Rosanne Boudreau, Ryan H Rochat, Michael F Schmid, Yang Xia, Carolyn A Larabell, and Wah Chiu. Visualizing red blood cell sickling and the effects of inhibition of sphingosine kinase 1 using soft x-ray tomography. *Journal of cell science*, 129(18):3511–3517, 2016.

[4] Patricia Yang Liu, LK Chin, W Ser, HF Chen, C-M Hsieh, C-H Lee, K-B Sung, TC Ayi, PH Yap, B Liedberg, et al. Cell refractive index for cell biology and disease diagnosis: past, present and future. *Lab on a Chip*, 16(4):634–644, 2016.

[5] Metin N Gurcan, Laura E Boucheron, Ali Can, Anant Madabhushi, Nasir M Rajpoot, and Bulent Yener. Histopathological image analysis: A review. *IEEE reviews in biomedical engineering*, 2:147–171, 2009.

[6] Ronald E Gordon. Electron microscopy: a brief history and review of current clinical application. *Histopathology: Methods and Protocols*, pages 119–135, 2014.

[7] Maria Harkiolaki, Michele C Darrow, Matthew C Spink, Ewelina Kosior, Kyle Dent, and Elizabeth Duke. Cryo-soft x-ray tomography: using soft x-rays to explore the ultrastructure of whole cells. *Emerging topics in life sciences*, 2(1):81–92, 2018.

[8] Valentina Loconte, Jian-Hua Chen, Mirko Cortese, Axel Ekman, Mark A Le Gros, Carolyn Larabell, Ralf Bartenschlager, and Venera Weinhardt. Using soft x-ray tomography for rapid whole-cell quantitative imaging of sars-cov-2-infected cells. *Cell reports methods*, 1(7):100117, 2021.

[9] Michael CA Dyhr, Mohsen Sadeghi, Ralitsa Moynova, Carolin Knappe, Burcu Kepsutlu, Stephan Werner, Gerd Schneider, James McNally, Frank Noé, and Helge Ewers. 3d-surface reconstruction of cellular cryo-soft x-ray microscopy tomograms using semi-supervised deep learning. *bioRxiv*, pages 2022–05, 2022.

[10] Valentina Loconte, Jitin Singla, Angdi Li, Jian-Hua Chen, Axel Ekman, Gerry McDermott, Andrej Sali, Mark Le Gros, Kate L White, and Carolyn A Larabell. Soft x-ray tomography to map and quantify organelle interactions at the mesoscale. *Structure*, 30(4):510–521, 2022.

[11] Valentina Loconte, Jian-Hua Chen, Bieke Vanslembrouck, Axel A Ekman, Gerry McDermott, Mark A Le Gros, and Carolyn A Larabell. Soft x-ray tomograms provide a structural basis for whole-cell modeling. *The FASEB Journal*, 37(1):e22681, 2023.

[12] Gerd Schneider, Peter Guttmann, Stefan Heim, Stefan Rehbein, Florian Mueller, Kunio Nagashima, J Bernard Heymann, Waltraud G Müller, and James G McNally. Three-dimensional cellular ultrastructure resolved by x-ray microscopy. *Nature methods*, 7(12):985–987, 2010.

[13] Kamal L Nahas, João Ferreira Fernandes, Nina Vyas, Colin Crump, Stephen Graham, and Maria Harkiolaki. Contour: A semi-automated segmentation and quantitation tool for cryo-soft-x-ray tomography. *Biological imaging*, 2:e3, 2022.

[14] Kamal L Nahas, Viv Connor, Katharina M Scherer, Clemens F Kaminski, Maria Harkiolaki, Colin M Crump, and Stephen C Graham. Near-native state imaging by cryo-soft-x-ray tomography reveals remodelling of multiple cellular organelles during hsv-1 infection. *PLoS Pathogens*, 18(7):e1010629, 2022.

[15] Antoine Cossa, Sylvain Trépout, Frank Wien, Johannes Groen, Etienne Le Brun, Florian Turbant, Laetitia Besse, Eva Pereiro, and Véronique Arluison. Cryo soft x-ray tomography to explore escherichia coli nucleoid remodeling by hfq master regulator. *Journal of Structural Biology*, 214(4):107912, 2022.

[16] Carla C Polo, Miriam H Fonseca-Alaniz, Jian-Hua Chen, Axel Ekman, Gerry McDermott, Florian Meneau, José E Krieger, and Ayumi A Miyakawa. Three-dimensional imaging of mitochondrial cristae complexity using cryo-soft x-ray tomography. *Scientific reports*, 10(1):21045, 2020.

[17] Ignacio Arganda-Carreras, Verena Kaynig, Curtis Rueden, Kevin W Eliceiri, Johannes Schindelin, Albert Cardona, and H Sebastian Seung. Trainable weka segmentation: a machine learning tool for microscopy pixel classification. *Bioinformatics*, 33(15):2424–2426, 2017.

[18] John Paul Francis, Hongzhi Wang, Kate White, Tanveer Syeda-Mahmood, and Raymond Stevens. Neural network segmentation of cell ultrastructure using incomplete annotation. In *2020 IEEE 17th International Symposium on Biomedical Imaging (ISBI)*, pages 1183–1187. IEEE, 2020.

[19] Jacob Egebjerg, Maria Szomek, Katja Thaysen, Alice Dupont Juhl, Christoph Pratsch, Stephan Werner, Gerd Schneider, Richard Rottger, and Daniel Wustner. Automated quantification of lipophagy in saccharomyces cerevisiae from fluorescence and cryo-soft x-ray microscopy data using deep learning. *bioRxiv*, pages 2023–02, 2023.

[20] Angdi Li, Xiangyi Zhang, Jitin Singla, Kate White, Valentina Loconte, Chuanyang Hu, Chuyu Zhang, Shuailin Li, Weimin Li, John Paul Francis, et al. Auto-segmentation and time-dependent systematic analysis of mesoscale cellular structure in β-cells during insulin secretion. *Plos one*, 17(3):e0265567, 2022.

[21] Philipp Lösel and Vincent Heuveline. Enhancing a diffusion algorithm for 4d image segmentation using local information. In *Medical Imaging 2016: Image Processing*, volume 9784, pages 707–717. SPIE, 2016.

[22] Philipp D Lösel, Thomas van de Kamp, Alejandra Jayme, Alexey Ershov, Tomáš Faragó, Olaf Pichler, Nicholas Tan Jerome, Narendar Aadepu, Sabine Bremer, Suren A Chilingaryan, et al. Introducing biomedisa as an open-source online platform for biomedical image segmentation. *Nature communications*, 11(1):5577, 2020.

[23] Kenneth Fahy, Tony McEnroe, Fergal O'Reilly, William Fyans, Dunja Skoko, and Paul Sheridan. Development of a commercial laboratory scale soft x-ray microscope. *Microscopy and Microanalysis*, 26(S2):3008–3009, 2020.

[24] Mark A Le Gros, Gerry McDermott, Bertrand P Cinquin, Elizabeth A Smith, Myan Do, Weilun L Chao, Patrick P Naulleau, and Carolyn A Larabell. Biological soft x-ray tomography on beamline 2.1 at the advanced light source. *Journal of synchrotron radiation*, 21(6):1370–1377, 2014.

[25] Venera Weinhardt, Jian-Hua Chen, Axel A Ekman, Jessica Guo, Soumya G Remesh, Michal Hammel, Gerry McDermott, Weilun Chao, Sharon Oh, Mark A Le Gros, et al. Switchable resolution in soft x-ray tomography of single cells. *PLoS One*, 15(1):e0227601, 2020.

[26] Dilworth Y Parkinson, Christian Knoechel, Chao Yang, Carolyn A Larabell, and Mark A Le Gros. Automatic alignment and reconstruction of images for soft x-ray tomography. *Journal of structural biology*, 177(2):259–266, 2012.

[27] Jian-Hua Chen, Bieke Vanslembrouck, Valentina Loconte, Axel Ekman, Mirko Cortese, Ralf Bartenschlager, Gerry McDermott, Carolyn A Larabell, Mark A Le Gros, and Venera Weinhardt. A protocol for full-rotation soft x-ray tomography of single cells. *STAR protocols*, 3(1):101176, 2022.

[28] The pancreatic β-cell consortium.

[29] Andriy Fedorov, Reinhard Beichel, Jayashree Kalpathy-Cramer, Julien Finet, Jean-Christophe Fillion-Robin, Sonia Pujol, Christian Bauer, Dominique Jennings, Fiona Fennessy, Milan Sonka, et al. 3d slicer as an image computing platform for the quantitative imaging network. *Magnetic resonance imaging*, 30(9):1323–1341, 2012.

[30] Ron Kikinis, Steve D Pieper, and Kirby G Vosburgh. 3d slicer: a platform for subject-specific image analysis, visualization, and clinical support. In *Intraoperative imaging and image-guided therapy*, pages 277–289. Springer, 2013.

[31] Özgün Çiçek, Ahmed Abdulkadir, Soeren S Lienkamp, Thomas Brox, and Olaf Ronneberger. 3d u-net: learning dense volumetric segmentation from sparse annotation. In *Medical Image Computing and Computer-Assisted Intervention–MICCAI 2016: 19th International Conference, Athens, Greece, October 17-21, 2016, Proceedings, Part II 19*, pages 424–432. Springer, 2016.

[32] Takafumi Nemoto, Natsumi Futakami, Etsuo Kunieda, Masamichi Yagi, Atsuya Takeda, Takeshi Akiba, Eride Mutu, and Naoyuki Shigematsu. Effects of sample size and data augmentation on u-net-based automatic segmentation of various organs. *Radiological Physics and Technology*, 14:318–327, 2021.

[33] Philipp D Lösel, Coline Monchanin, Renaud Lebrun, Alejandra Jayme, Jacob Relle, Jean-Marc Devaud, Vincent Heuveline, and Mathieu Lihoreau. Natural variability in bee brain size and symmetry revealed by micro-ct imaging and deep learning. *bioRxiv*, pages 2022–10, 2022.

[34] Lena Maier-Hein, Matthias Eisenmann, Annika Reinke, Sinan Onogur, Marko Stankovic, Patrick Scholz, Tal Arbel, Hrvoje Bogunovic, Andrew P Bradley, Aaron Carass, et al. Why rankings of biomedical image analysis competitions should be interpreted with care. *Nature communications*, 9(1):5217, 2018.

[35] Lena Maier-Hein, Bjoern Menze, et al. Metrics reloaded: Pitfalls and recommendations for image analysis validation. *arXiv. org*, (2206.01653), 2022.

[36] Matthew B Smith, Guillaume Salbreux, Christopher Dunsby, Hugh Sparks, Jorge Almagro, Axel Behrens, and Agathe Chaigne. Active mesh and neural network pipeline for cell aggregate segmentation. *bioRxiv*, pages 2023–02, 2023.

Preprint Series of the Engineering Mathematics and Computing Lab

recent issues

No. 2023-01 Marco Schröder, Stefan Machmeier, Vincent Heuveline: Vtable hijacking: Object Type Integrity for run-time type information

No. 2021-02 Alejandra Jayme, Philipp D. Lösel, Joachim Fischer, Vincent Heuveline: Comparison of Machine Learning Methods for Predicting Employee Absences

No. 2021-01 Chen Song, Jonas Roller, Ana Victoria Ponce-Bobadilla, Nicolas Palacio-Escat, Julio Saez-Rodriguez, Vincent Heuveline: Spatial Effect on Separatrix of Two-Cell System and Parameter Sensitivity Analysis

No. 2020-01 Saskia Haupt, Nassim Fard-Rutherford, Philipp D. Lösel, Lars Grenacher, Arianeb Mehrabi, Vincent Heuveline: Mathematical Clustering Based on CrossSections in Medicine: Application to the Pancreatic Neck

No. 2019-02 Nils Schween, Nico Meyer-H übner, Philipp Gerstner, Vincent Heuveline: A time stepreduction method for Multi-Period Optimal Power Flow problems

No. 2019-01 Philipp Gerstner, Martin Baumann, Vincent Heuveline: Analysis of the StationaryThermal-Electro Hydrodynamic Boussinesq Equations

No. 2018-02 Simon Gawlok, Vincent Heuveline: Nested Schur-Complement Solver for a Low-MachNumber Model: Application to a Cyclone-Cyclone Interaction

No. 2018-01 David John, Michael Schick, Vincent Heuveline: Learning model discrepancy of anelectric motor with Bayesian inference

No. 2017-06 Simon Gawlok, Philipp Gerstner, Saskia Haupt, Vincent Heuveline, Jonas Kratzke, Philipp Lösel, Katrin Mang, Maraike Schmidtobreick, Nicolai Schoch, Nils Schween, Jonathan Schwegler, Chen Song, Marin Wlotzka: HiFlow3 Technical Report on Release 2.0

No. 2017-05 Nicolai Schoch, Vincent Heuveline: Towards an Intelligent Framework for Personalized Simulation-enhanced Surgery Assistance: Linking a Simulation Ontology to a Reinforcement Learning Algorithm for Calibration of Numerical Simulations

No. 2017-04 Martin Wlotzka, Thierry Morel, Andrea Piacentini, Vincent Heuveline: New features for advanced dynamic parallel communication routines in OpenPALM: Algorithms and documentation

No. 2017-03 Martin Wlotzka, Vincent Heuveline: An energy-efficient parallel multigrid method for multi-core CPU platforms and HPC clusters

No. 2017-02 Thomas Loderer, Vincent Heuveline: New sparsing approach for real-time simulations of stiff models on electronic control units

No. 2017-01 Chen Song, Markus Stoll, Kristina Giske, Rolf Bendl, Vincent Heuveline: Sparse Gridsfor quantifying motion uncertainties in biomechanical models of radiotherapy patients

No. 2016-02 Jonas Kratzke, Vincent Heuveline: An analytically solvable benchmark problem for fluid-structure interaction with uncertain parameters

Preprint Series of the Engineering Mathematics and Computing Lab (EMCL)

www.emcl.iwr.uni-heidelberg.de